Please cite the Published Version

Additional Information: This is an open access article which first appeared in Applied Materials Today

Data Access Statement: Data will be made available on request.

Contents lists available at ScienceDirect

Applied Materials Today

journal homepage: www.elsevier.com/locate/apmt

Gold nanoparticle infused castor oil for the production of high performance conductive additive manufacturing filament

Elena Bernalte [a], Robert D. Crapnell [a], Rania El Azizi [a,b], Karen K.L. Augusto [a,c], Craig E. Banks [a,*]

[a] Faculty of Science and Engineering, Manchester Metropolitan University, Dalton Building, Chester Street, M1 5GD, Great Britain.
[b] Department of Physical Measurements, Sorbonne Paris North University, Place du 8 Mai 1945, 93200, Saint-Denis, France
[c] Laboratório de Analítica, Bioanalítica, Biosensores, Electroanalítica e Sensores, Departamento de Química, Universidade Federal de São Carlos (UFSCar), CP 676, 13560-970 São Carlos-SP, Brazil

ARTICLE INFO

ABSTRACT

The development of high-performance, bespoke conductive filament is a challenge to overcome to increase the uptake of additive manufacturing electrochemistry. In this work we report the first conductive filament embedded with gold nanoparticles (AuNPs). This is achieved through the synthesis of AuNPs within castor oil (AuNP-CO), a recognised plasticiser used to fabricate bespoke conductive filaments. The presence of AuNPs in castor oil is first confirmed through UV–Vis and TEM measurements and after the AuNP-CO is utilised as a substitute for CO within a filament composition comprising of 25 wt% carbon black, 65 wt% recycled PLA and 10 wt% AuNP-CO. The inclusion of AuNP-CO provided both enhanced electrical properties, as well as low-temperature flexibility, without compromising on the thermal stability. This filament was shown to have excellent printability, with the presence of AuNPs confirmed on the surface of the additively manufactured electrodes. The electrodes containing AuNP-CO were benchmarked against only CO containing ones and a commercial alternative, whereby the AuNP-CO electrodes provided enhanced electrochemical performance toward both outer and inner sphere redox probes. Additionally, the AuNP-CO electrodes were shown to have significantly enhanced electroanalytical properties toward the detection of dopamine, showing double the sensitivity. We expect this first report of precious metal nanoparticle embedded conductive filament will broaden the scope of additive manufacturing in electrochemistry and significantly increase the potential for commercially viable products to emerge from this field.

1. Introduction

The production of novel, bespoke and highly conductive filament for additive manufacturing is of great interest across many industrial and academic sectors [1]. There are many techniques that fall under the umbrella of additive manufacturing, however one of the lowest cost of entries (and therefore attractive) is for Fused Filament Fabrication (FFF), also known as Fused Deposition Modelling (FDM). This methodology operates by extruding and depositing thermoplastic material in consecutive, thin-layered cross-sections, culminating in the production a final 3-dimensional structure. FFF enables the rapid creation of bespoke parts with complex geometries, offering high customisability, low production costs and significantly reduced waste compared to traditional formative or subtractive manufacturing techniques. Additionally,

additive manufacturing offers globally connected production, allowing designs and files to be sent and printed anywhere in the world. Due to these various reasons, the uptake of FFF has been high.

One emerging area within FFF is the application of additive manufacturing in electrochemistry. The combination of commercially available conductive filament and the current low-cost of good quality printers, in addition to the advantages mentioned above, have increasingly encouraged electrochemists to explore this area. However, although conductive, the electrochemical performance of the commercial filament is poor, and researchers have spent significant amounts of time attempting to improve this whether optimising the design/printing parameters [2] or activating the electrodes [3] with relative success. Even so, the performance is still substantially substandard for additively manufactured electrodes to compete with classical electrodes such as

---

glassy carbon, boron-doped diamond, or even screen-printed electrodes. As such, researchers have recently began producing their own bespoke filament, allowing them to precisely control the conductive filler content [4]. This started with the inclusion of carbon black (CB) in higher loadings than reported in the commercial filament, providing significantly enhanced electrochemical performance for energy storage [5] and electroanalysis [6]. More recently, research has expanded into using combinations of carbon allotropes in order to synergise their properties, such as combining multi-walled carbon nanotubes (MWCNT) and CB for enhanced conductivity [7] or through utilising graphite and CB to maintain performance but lower the material cost [8].

These last reports are also examples of a great effort from researchers to consider the environmental aspects of the filament by moving away from petrochemical based carbon sources. Moreover, the sustainability of conductive filaments has been an important area of research [9], whereby reports aiming toward a circular economy electrochemistry showed that conductive filament could be produced from coffee-pod waste for the detection of caffeine [10]. This concept was taken further to show that already used electroanalytical sensors could be recycled into a new device, even if mixed material prints were used [11]. In addition to the carbon source and transition to recycled plastics [12], researchers have looked to improve the sustainability of the plasticiser within the bespoke filaments. The International Union of Pure and Applied Chemistry (IUPAC) defines a plasticiser as "*a substance incorporated into a material to increase its flexibility, workability, or distensibility*" [13]. Initial reports of bespoke conductive filaments used poly(ethylene glycol) (PEG) [5,14] or poly(ethylene succinate) [10] as plasticisers, but these compounds commonly require the use of organometallic catalysts within their production. Alternatively, researchers have postulated the use of a bio-based compound, namely castor oil [15]. This was shown to offer excellent low-temperature flexibility to the filament, whilst offering low capacitance resolving the issue when filaments containing PEG were applied for electroanalysis.

The drive for improved electrochemical performance whilst not impacting the sustainability or biocompatibility of the filament has led to an interest in gold nanoparticles (AuNPs). Although there have been reports of AuNPs on additively manufactured electrodes, these examples predominantly involved the post-print modification of the surface through electrodeposition or electroplating [16], as established in the literature for solid [17] or screen-printed [18] electrodes. However, to maximise the manufacturing process and performance of 3D printed electrodes, the metallic nanoparticles should be embedded within the filament. In this regard, the synthesis of AuNPs within castor oil as reported by da Silva et al. [19] is an intriguing proposition. In this work, the authors synthesise colloidal nanoparticles which are directly dispersed within castor oil using different methodologies. In this work, we selected the reaction performed in alkaline media where a solution with aqueous components for the AuNPs synthesis was mixed with castor oil, and ethanol to help facilitate the transfer of the AuNPs from the aqueous phase to the oil phase [20]. This intriguing approach could allow for the castor oil to contribute dual-functionality within the filament, both improving the electrochemical performance and low-temperature flexibility.

In this work, we propose the synthesis of AuNPs within castor oil, followed by the production of highly conductive additive manufacturing filament from recycled poly(lactic acid) (PLA). The combination of both conductive carbon nanofiller and AuNPs will enhance the performance of the filament, whilst also not requiring post-print modification to incorporate the nanoparticles. We believe this work introduces a step-change in the way conductive additive manufacturing filament can be produced and opens a wide variety of new fields of exploration for the area of additive manufacturing electrochemistry.

2. Experimental section

2.1. Chemicals

All chemicals used throughout this work were used as received without any further purification. All aqueous solutions were prepared with deionised water of a measured resistivity not less than 18.2 MΩ cm, sourced from a Milli-Q Integral 3 system from Millipore UK (Watford, UK). Hexaammineruthenium (III) chloride (98 %), castor oil (98 %), potassium ferricyanide (99 %), potassium ferrocyanide (98.5–102 %), sodium hydroxide (>98 %), potassium chloride (99.0–100.5 %), gold (III) chloride trihydrate (≥99.9 %), dopamine hydrochloride (98 %), potassium hydroxide (99.99 %), ethanol absolute (Pure, 200 proof) and phosphate-buffered saline (PBS) tablets were purchased from Merck (Gillingham, UK). Carbon black was purchased from PI-KEM (Tamworth, UK). Recycled poly(lactic acid) (rPLA) was purchased from Gianeco (Turin, Italy). Commercial conductive PLA/carbon black filament (1.75 mm, ProtoPasta, Vancouver, Canada) was purchased from Farnell (Leeds, UK).

2.2. Synthesis of AuNPs in CO

To synthesise the AuNPs, CO (10 mL), ethanol (10 mL), gold (III) chloride trihydrate (2 mL, 30 mM aqueous solution), and potassium hydroxide (KOH) (1 mL, 0.1 M aqueous) were added to a 100 mL round bottom flask. The solution was stirred vigorously at room temperature until a greyish/black suspension was observed (~15 min). After this, the solution was set to reflux at 80 °C for 24 h, whereby the solution changes to a red colour. The oil phase was then decanted from the biphasic mixture, washed further with water (10 mL), and separated again. Finally, the separated oil phase was centrifuged, and remaining water drops separated using a pipette. The AuNP-CO is then ready to use.

2.3. Recycled filament production

All rPLA was dried in an oven at 60 °C for a minimum of 2.5 h before use to remove any residual water in the polymer. The polymer compositions were prepared through the addition of appropriate amounts of rPLA (65 wt%), CB (25 wt%), and either CO or AuNP-CO (10 wt%) in a chamber of 63 cm^3. The compounds were mixed using a Thermo Haake Polydrive dynameter fitted with a Thermo Haake Rheomix 600 (Thermo-Haake, Germany) at 190 °C with Banbury rotors at 70 rpm for 5 min. The resulting polymer composites were allowed to cool to room temperature before being granulated to create a finer particle size using a Rapid Granulator 1528 (Rapid, Sweden). The polymer composites were collected and processed through the hopper of a EX2 extrusion line (Filabot, VA, United States). The EX2 was set up with a single screw with a heat zone of 195 °C. The molten polymer was extruded from a 1.75 mm die head, pulled along an Airpath cooling line (Filabot, VA, United States) and collected on a spool. After which the filament was then ready to use for Additive Manufacturing (AM).

2.4. Additive manufacturing of the electrodes

All computer designs and 3MF files in this manuscript were produced using Fusion 360® (Autodesk®, CA, United States). These files were sliced and converted to GCODE files in PrusaSlicer (Prusa Research, Prague, Czech Republic). The additive manufactured electrodes were produced using fused filament fabrication (FFF) technology on a Prusa i3 MK3S+ (Prusa Research, Prague, Czech Republic). All additive manufactured electrodes were printed using identical printing parameters, namely a 0.6 mm nozzle with a nozzle temperature of 215 °C, 100 % rectilinear infill [2a], 0.15 mm layer height, and print speed of 35 mm s^{-1}. Electrodes were printed on smooth PEI steel sheet heated up at 50 °C, without additional conditioning.

2.5. Physicochemical characterisation

Scanning Electron Microscopy (SEM) micrographs were obtained using a Crossbeam 350 Focussed Ion Beam – Scanning Electron Microscope (FIB-SEM) (Carl Zeiss Ltd., Cambridge, UK) fitted with a field emission electron gun. Secondary electron imaging was completed using a Secondary Electron Secondary Ion (SESI) detector. Samples were mounted on the aluminium SEM pin stubs (12 mm diameter, Agar Scientific, Essex, UK) using adhesive carbon tabs (12 mm diameter, Agar Scientific, Essex, UK) and coated with a 5 nm layer of Au/Pd metal using a Leica EM ACE200 coating system before imaging.

Transmission Electron Microscopy (TEM) was performed at University of Nottingham (UK). The sample was deposited onto a Cu 300 mesh graphene oxide support grid (EMResolutions) and washed with hexane to remove the castor oil. After drying overnight under vacuum, the sample was imaged on a JEOL 2100F TEM, operating at 200 kV equipped with a Gatan K3 direct electron camera. An objective aperture and nominal under focus conditions were applied. Images were collected in three separate regions of the TEM grid.

Thermogravimetric analysis (TGA) was performed using a Discovery Series SDT 650 controlled by Trios Software (TA Instruments, DA, USA). Samples made of pieces of filament were mounted in alumina pans (90 μL) and tested using a ramp profile (10 °C min^{-1}) from 0 – 800 °C under N$_2$ (100 mL min^{-1}).

X-ray diffraction (XRD) measurements were performed on the 3D printed electrodes using only castor oil and AuNPs in castor oil as plasticiser, respectively, to obtain the structural information using PANalytical X'Pert Powder X-ray diffractometer with Cu ($\lambda = 1.54$ Å) as the source with 45 kV voltage and 40 mA current settings. The data were collected in a continuous mode over the 2Θ scan range of 5° – 90°, with a step size of 0.01° for 108 s per step at room temperature under ambient conditions. The samples were spinning at 16 rpm during the measurements for uniform data collection. PreFIX module on the incident beam side with the automatic divergence and fixed anti-scatter slit of 4° along with PreFIX module on the diffracted side with PIXcel 1D detector in scanning line mode with programmable anti-scatter slit were used to collect the diffraction patterns from a constant irradiated length of 0.5 mm.

2.6. Electrochemical experiments

All electrochemical experiments were performed on an Autolab 100 N potentiostat controlled by NOVA 2.1.7 (Utrecht, The Netherlands). Identical additive manufactured electrodes were used throughout this work for all filaments, printed in a lollipop shape (Ø 5 mm disc with a connection stem of 8 mm connection length, 2 mm width and 1 mm thickness [2b]) (Figure S1A) alongside an external commercial Ag|AgCl/KCl (3M) reference electrode with a nichrome wire counter electrode. All solutions of [Ru(NH$_3$)$_6$]$^{3+}$ were purged of O$_2$ thoroughly using N$_2$ prior to any electrochemical experiments. Solutions of [Fe(CN)$_6$]$^{4-/3-}$ were prepared in the same way without the need of further degassing.

Electrochemical impedance spectroscopy (EIS) was recorded in the frequency range 0.1 Hz to 100 kHz applying 10 mV of signal amplitude to perturb the system under quiescent conditions. NOVA 2.1.7 software was used to fit Nyquist plots obtained to adequate equivalent circuit.

Activation of the additive manufactured electrodes was performed, where applicable, electrochemically in NaOH (0.5 M), as described in the literature [21]. Briefly, the additive manufactured electrodes were connected as the working electrode in conjunction with a nichrome wire coil counter and Ag|AgCl/KCl (3 M) reference electrode and placed in a solution of 0.5 M NaOH. Chronoamperometry was used to activate the additive manufactured electrodes by applying a set voltage of $+ 1.4$ V for 200 s, followed by applying $- 1.0$ V for 200 s. The additive manufactured electrodes were then thoroughly rinsed with deionised water and dried under compressed air before further use.

3. Results and discussion

3.1. Synthesis of gold nanoparticles (AuNPs) in castor oil and incorporation into filament

To enhance the electrochemical performance of electrically conductive additive manufacturing filament, we propose embedding AuNPs within the filament in addition to the conductive carbon allotropes. We look to achieve this through the combination of synthesis of AuNPs within castor oil to create AuNPs modified CO (AuNP-CO), followed by the use of this as the plasticiser within conductive recycled PLA filament, as described previously with unmodified CO [15].

To synthesise the AuNPs, a known technique using KOH and high temperatures to reduce Au(III) salts was applied. The nucleation of the highly charged AuNPs starts in the aqueous phase, the *a priori* not favoured transfer to the organic (oil) phase occurs in the first 2 h of the reaction, leading to stable colloids of AuNPs in castor oil [19]. The unique physicochemical properties of CO and its role as green source of capping agent in nanoparticles' syntheses is attributed to its main constituent, ricinoleic acid [20,22] — an 18-carbon fatty acid that contains a hydroxyl group at the carbon 12 (Figure S2). According to the literature, due to the presence of hydrogen bonds between such hydroxyl groups present in the molecular structure of the castor oil and the oxygenated negatively charged groups that surround the AuNPs synthesised in KOH, the colloidal stabilisation of the AuNPs in castor oil occurs [19]. Thus, the colour change accompanying the synthesis of the AuNPs in CO from pale yellow/colourless to a reddish solution is illustrated in Fig. 1A and 1B, where a comparison between the pure castor oil and the modified CO is presented.

The UV–Vis absorption spectra obtained for the AuNP-CO solution is presented in Fig. 1C, where a clear peak is observed that is centred at 535 nm, showing good agreement with previous reports for AuNPs in this environment [19,20].To confirm the presence of AuNPs TEM analysis was performed, Fig. 2, where it can be seen that spherical colloidal AuNPs were present in the system at ~30 nm in size.

Once the presence of AuNPs was confirmed within the CO, this AuNP-CO was utilised for the production of conductive additive manufacturing filament. Previously, CO has been used as a plasticiser with 25 wt% of CB within recycled PLA, and as such we use this as a benchmark (alongside a commercially available conductive PLA filament) for our modified AuNP-CO. The new filament was produced in the same way, using the thermal mixing methodology [4] described in the Section 2.3. There was no discernible difference in the low-temperature flexibilities between the CO filament and the AuNP-CO filament, indicating that both would have good printability (Figure S1B and S1C). Thermogravimetric analysis was performed on the filaments, Fig. 3A, where there is no significant change in the onset of degradation temperature. The CO filament produced an onset temperature of 283 ± 4 °C, while the AuNP-CO filament had a value of 281 ± 3 °C, which indicated that the inclusion of AuNPs did not have a negative effect on the temperature resistance of the filament. It can be seen that both the modified filaments have a higher onset temperature than pure castor oil, indicating that once mixed into the polymer composite some stabilisation is observed. Using TGA, the actual filler content of the filaments was also confirmed, which corresponded to 23 ± 2 wt% and 25 ± 2 wt% for the CO and AuNP-CO filaments, respectively. As with previous work, the bulk resistance across 10 cm of filament was measured as this allows benchmarking to other bespoke filaments, as well as the commercial conductive PLA. The AuNP-CO filament produced a resistance across 10 cm of 644 ± 25 Ω, which shows an improvement, presumably due to the presence of highly conductive AuNPs, compared to the only CO filament of 864 ± 54 Ω [15], and the commercial conductive PLA of 2–3 kΩ. Following this, the filaments were used to print additively manufactured electrodes to benchmark their electrochemical responses.

Within Fig. 3B is an SEM micrograph showing the surface of the additively manufactured electrode, where a large concentration of
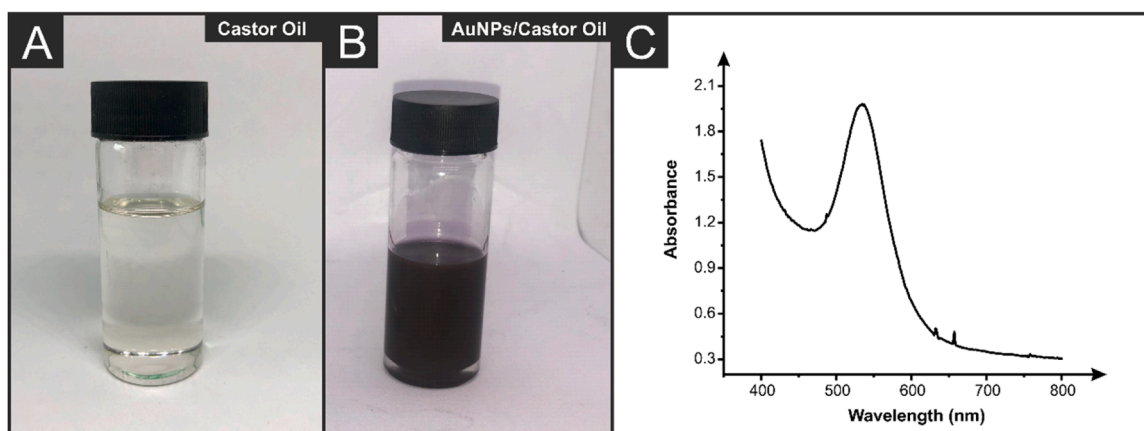
Fig. 1. Photographs of the **A)** unmodified castor oil, and **B)** AuNPs modified castor oil. **C)** UV–Vis spectra obtained for the AuNPs modified castor oil.
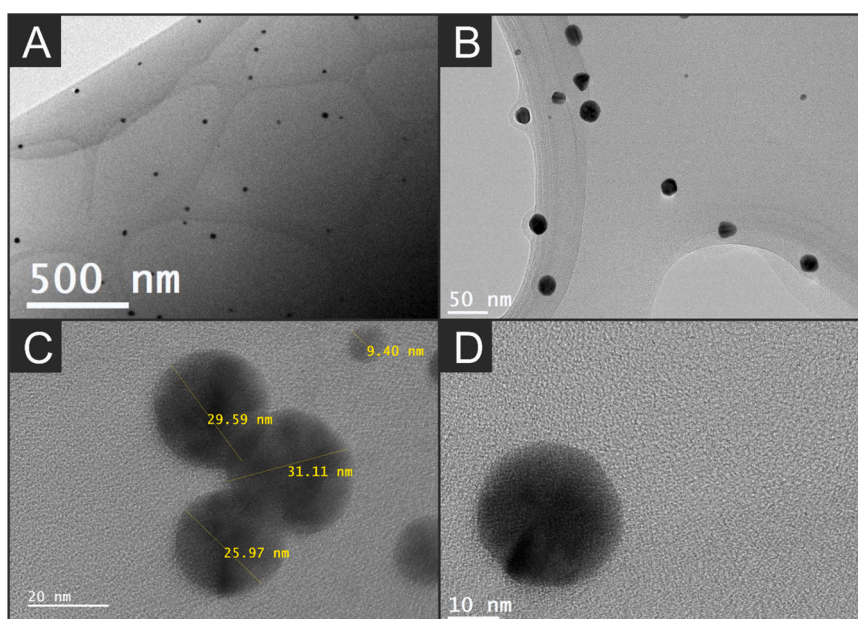

**Fig. 2.** TEM images for the synthesised AuNPs.

spherical CB particles can be observed, with areas of polymer in between. The availability of the CB indicates that the electrode would perform well for electrochemical reactions; however, due to the particle size and shape of CB it is difficult to confirm the presence of AuNPs through this method. As such, EDX was applied, Fig. 3C-E, where sample mapping indicated the presence of Au on the surface of the additively manufactured electrode. It is noted that the concentration of AuNPs is expected to be low as the AuNP-CO only makes up 10 wt% of the filament, and the AuNPs are only a fraction of this 10 wt%. Finally, X-ray diffraction analysis on the additively manufactured electrode fabricated using AuNP-CO were carried out (Figure S3). It can be observed that the material displays a broad peak between 2θ angles of 10 to 25°, which is due to the scattering of the poorly crystalline matrix of rPLA [23]. Additionally, the expected small diffraction peaks that could be detected on the AuNP-CO electrode appeared at 38.3°, 44.4°, and 77.7°, corresponding to (111), (200) and (311) planes of Au, respectively (JCPDS No. 04–0784) [24]. After confirming the successful production of filament and additively manufactured electrodes from the AuNP-CO, we now look to electrochemically characterise the electrodes.

3.2. Electrochemical characterisation of the additive manufactured electrodes

Once physicochemically characterised, the electrochemical performance of the electrodes printed from AuNP-CO filament was explored and benchmarked against a bespoke CO filament prepared in the same way as reported previously [15], and the commercial conductive filament. The electrodes printed from these filaments were tested against both the near-ideal outer-sphere redox probe $[Ru(NH_3)_6]^{3+}$ (1 mM in 0.1 M KCl), and the commonly used inner-sphere probe $[Fe(CN)_6]^{4-}$ (1 mM in 0.1 M KCl). Scan rate studies against $[Ru(NH_3)_6]^{3+}$ (1 mM in 0.1 M KCl) are performed first, as they allow for the best determination of heterogeneous electron (charge) transfer rate constant (k^0) and the real electrochemical surface area (A_e) [25]. The cyclic voltammograms obtained from the scan rate study (5–500 mV s^{-1}) for the AuNP-CO electrode are presented in Fig. 4A, with an example for the CO filament and commercial filament shown in Figure S4. In all three cases the expected redox peaks are obtained for the one electron reduction and oxidation of $[Ru(NH_3)_6]^{3+}$ at ~ -0.2 V and ~ -0.1 V respectively. Within all graphs the inset shows the appropriate Randles-Ševčík plot, where the linearity in all cases confirms the diffusion-controlled nature of the redox process. Fig. 4B presents a comparison of the cyclic voltammograms obtained at
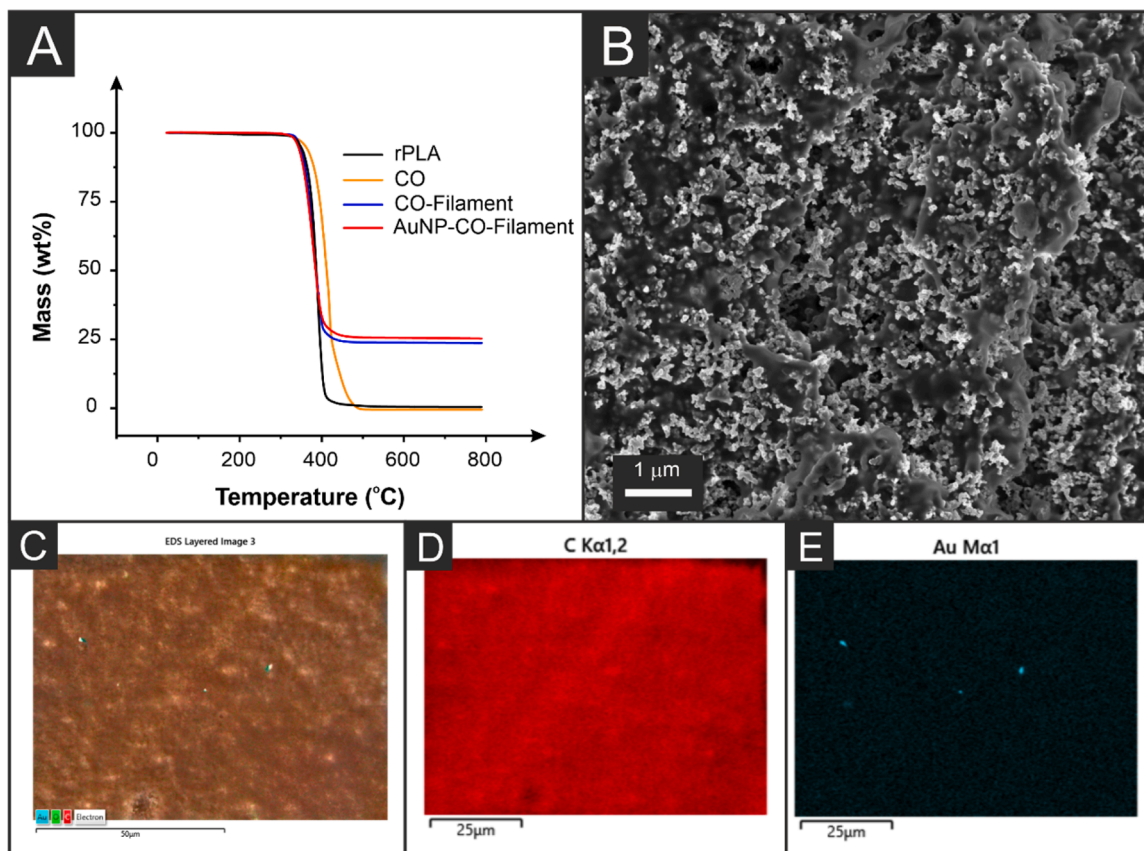
Fig. 3. A) Thermogravimetric analysis of the filaments. **B)** SEM micrograph of the surface of an additively manufactured electrode printed from the AuNP-CO filament. EDX surface mapping of an additively manufactured electrode surface with the **C)** layered image, **D)** carbon map, and **E)** gold map.
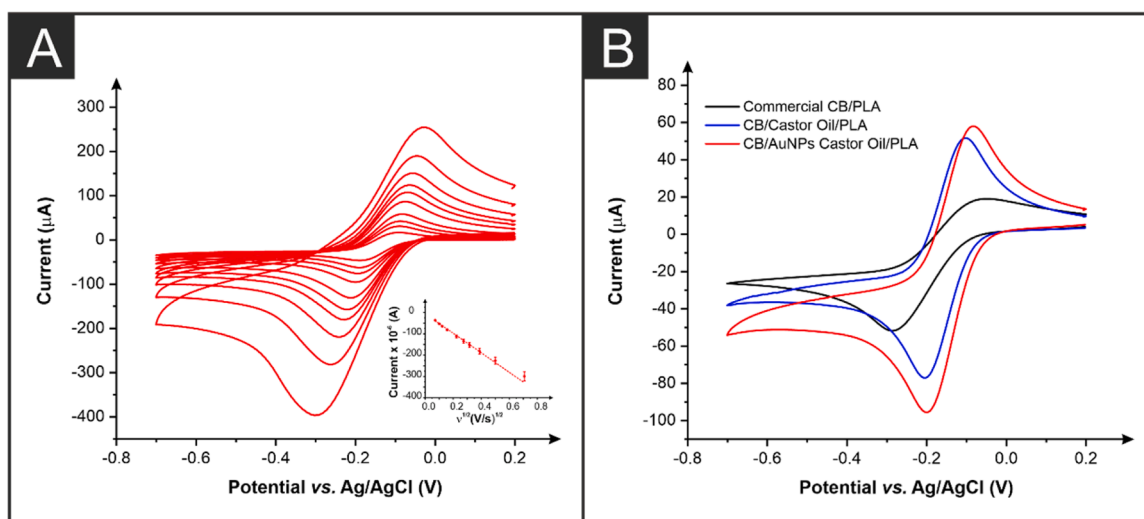
Fig. 4. A) Cyclic voltammograms (5 – 500 mV s^{-1}) of [Ru(NH$_3$)$_6$]$^{3+}$(1 mM in 0.1 M KCl), using an additively manufactured electrode printed from the AuNP-CO filament. **B)** Cyclic voltammograms (25 mV s^{-1}) of [Ru(NH$_3$)$_6$]$^{3+}$(1 mM in 0.1 M KCl) performed using additively manufactured electrodes printed from the AuNP-CO (red), CO (blue), and commercial (black) filaments.

25 mV s^{-1} for the AuNP-CO, CO, and commercial electrodes. It can be seen clearly that both bespoke filaments offer significant improvements over the commercial, in terms of peak current (I$_p$) and peak-to-peak separation (ΔE$_p$). The ΔE$_p$ improved from 250 mV for the commercial filament to 110 mV for both bespoke filaments, which highlights the significant improvement in electrochemical performance that can be obtained through bespoke filaments. Although there is no observed

improvement in the ΔE$_p$ for the AuNP-CO filament over the CO filament, there is a large increase in the measured peak current. This increased from 75 μA for the CO electrode to 95 μA for the AuNP-CO electrode, which shows a significant improvement attributed to the increased surface area provided by the AuNPs despite the overall low loading.

From the scan rate studies within [Ru(NH$_3$)$_6$]$^{3+}$ the $k°$ for each electrode was calculated as $1.48 \times 10^{-3} \pm 2.50 \times 10^{-4}$ cm s^{-1} for the

AuNP-CO, $1.94 \times 10^{-3} \pm 8.01 \times 10^{-4}$ cm s^{-1} for the CO, and $5.77 \times 10^{-4} \pm 7.63 \times 10^{-5}$ cm s^{-1} for the commercial. Clearly there is a large increase in the k^0 when moving from commercial filament to bespoke. For the A_e there is a large increase from the commercial filament at 0.34 ± 0.06 cm^2 to 0.46 ± 0.23 cm^2 for the CO bespoke, with a further increase to 0.61 ± 0.03 cm^2 for the AuNP-CO electrode. This increase in the electrochemical surface area is once more attributed to the presence of the AuNPs on the electrode.

Following analysis against [Ru(NH$_3$)$_6$]$^{3+}$, the electrodes were tested against the commonly used inner-sphere probe [Fe(CN)$_6$]$^{4-}$ (1 mM in 0.1 M KCl). The scan rate studies (5–500 mV s^{-1}) obtained for each electrode is provided in Figure S5. It is worth noting that the two peaks observed for the AuNP-CO responses in [Fe(CN)$_6$]$^{4-}$ (Figure S5C) evidences the presence of a mixed material with differences in their kinetics. Fig. 5A shows two sets of comparisons for the AuNP-CO (red), CO (blue) and commercial (black) electrodes. On the bottom is a comparison of as-printed electrodes toward [Fe(CN)$_6$]$^{4-}$ for each of these filaments, where it can be seen that essentially no redox process is seen for the commercial electrode. This response to inner sphere probes is expected for the commercial filament, which explains so much research that has been reported into improving the performance through either optimising the printing/design parameters [2a,2b,2d-f] or through activation of the electrode [3].

In contrast, both of the bespoke filaments show clear redox peaks for the [Fe(CN)$_6$]$^{4-}$ redox couple, although the ΔE_p values are significantly larger than ideal. It can be seen that the AuNP-CO electrode gives the best performance out of the as-printed electrodes in terms of both ΔE_p and I_p indicating that these electrodes have an improved electrochemical performance. This agrees with the intrinsic properties of this filament, where AuNPs infused in the CO plasticiser helps coat the CB particles in the structure of the filament, providing more natural reactivity towards the inner-sphere redox probe without the need of the electrode activation. When considering the activated electrodes, whereby the activation was electrochemically performed within NaOH (0.5 M) as described in the literature [21], there is a clear improvement in the electrochemical performance of all electrodes. The commercial electrode now produces a pair of redox peaks with a ΔE_p of ~500 mV, which is an improvement but still significantly worse than the bespoke electrodes that both produce values of ~350 mV. Additionally, both bespoke filaments provide a significant enhancement in the I_p compared to the commercial. It is interesting to note that the activation appears to have a more significant impact on the CO electrode than the AuNP-CO

electrode. The activated electrodes were then tested through electrochemical impedance spectroscopy, within [Fe(CN)$_6$]$^{4-/3-}$ (1 mM in 0.1 M KCl), with the associated Nyquist plot shown in Fig. 5B. From the Nyquist plot, both the solution resistance (R$_S$) and charge-transfer resistance (R$_{CT}$) can be established, which helps us understand the resistance introduced to the system by the additively manufactured electrode themselves and the resistance toward the electrochemical process occurring respectively. It can be seen that the expected semi-circular response is obtained for all three electrodes, however the magnitude of this is significantly reduced for the bespoke electrodes, hence a magnified inset is provided. Through appropriate fitting of the Nyquist plots, the R$_S$ for each electrode was obtained as 156 ± 1 Ω for the AuNP-CO, 199 ± 1 Ω for the CO, and 1121 ± 8 Ω for the commercial. The slight improvement obtained for the R$_S$ of the AuNP-CO bespoke filament compared to the CO filament and significant increase from the commercial filament is expected when considering the resistance values obtained from the raw filaments. When considering the R$_{CT}$ of the electrodes we observed that the AuNP-CO electrode performed the best, with a resistance of 274 ± 6 Ω, compared to 323 ± 5 Ω for the CO and 8914 ± 192 Ω. All this electrochemical data confirms that the inclusion of AuNPs within the castor oil plasticiser improves the electrochemical performance of the additively manufactured electrodes. We now look toward the response of the electrodes within an electroanalytical application.

3.3. Electroanalytical determination of dopamine

To observe how the electrochemical performance of additively manufactured electrodes printed from the AuNP-CO filament translates into the electroanalytical performance, tests were run against dopamine. Fig. 6A shows the first exploratory cyclic voltammograms (50 mV s^{-1}) performed for dopamine (1 mM in 0.01 M PBS, pH = 7.4), where the impressive performance of the AuNP-CO filament can be seen once again. There is an increase in the I_p as well as a significant reduction in the oxidation peak potential, which shows agreement with the excellent electrochemical kinetics seen earlier. It should be noted how the inclusion of such a low loading of AuNPs within the small volume of plasticiser compound improves the bespoke composition significantly.

These electrodes were then applied to the electroanalytical determination of dopamine, with the obtained calibration plots shown in Fig. 6B. It can clearly be seen that the AuNP-CO electrode produces the best results. Together with an impressive linearity displayed when
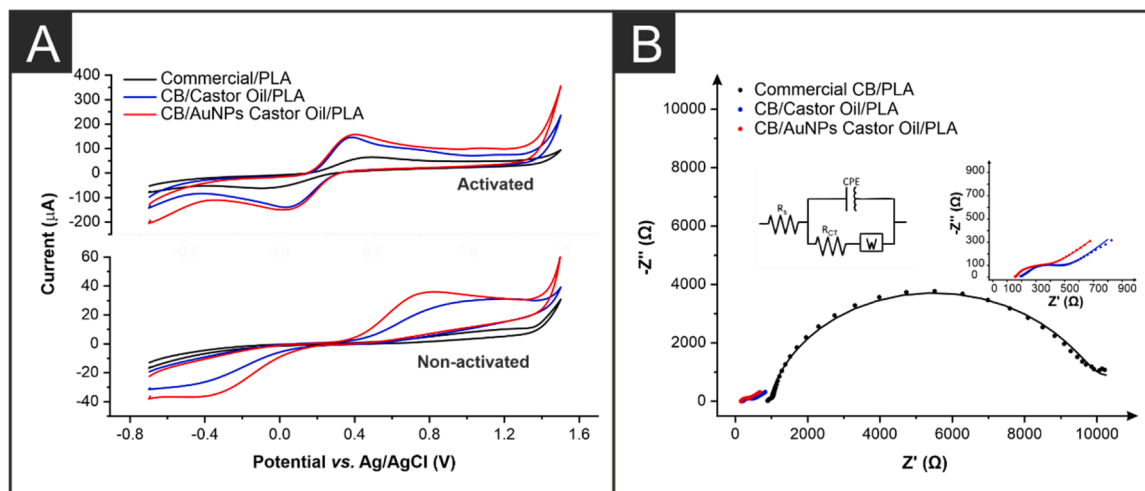
Fig. 5. A) Two plots (top = activated, bottom = as-print) of cyclic voltammograms (25 mV s^{-1}) of [Fe(CN)$_6$]$^{4-}$ (1 mM in 0.1 M KCl) performed using additively manufactured electrodes printed from the AuNP-CO (red), CO (blue), and commercial (black) filaments. **B)** Nyquist plots obtained through electrochemical impedance spectroscopy in [Fe(CN)$_6$]$^{4-/3-}$ (1 mM in 0.1 M KCl) performed using additively manufactured electrodes printed from the AuNP-CO (red), CO (blue), and commercial (black) filaments. Inset is a magnification of the two bespoke filaments.
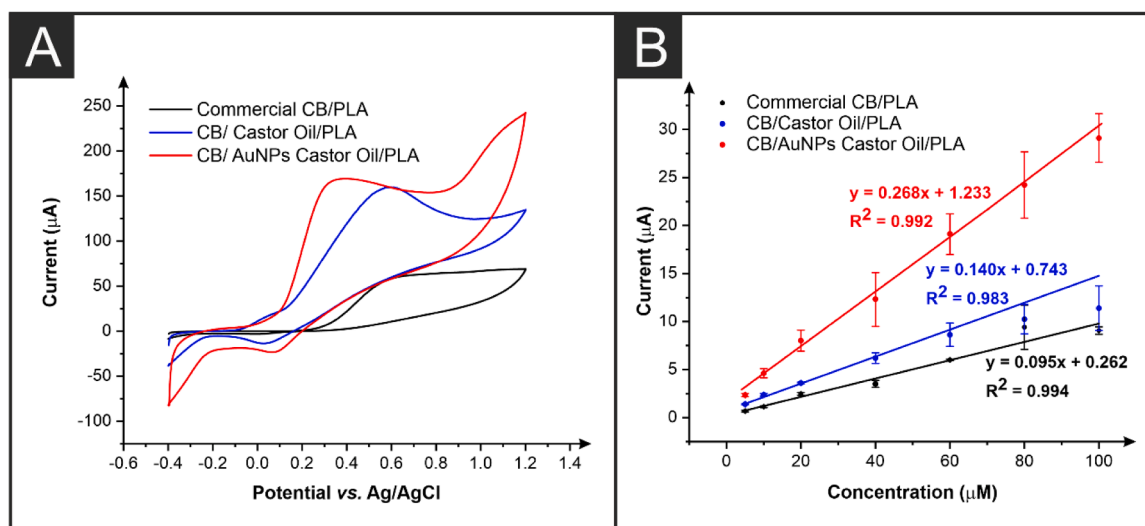
Fig. 6. A) Cyclic voltammogram (50 mV s^{-1}) for dopamine (1 mM in 0.01 M PBS, pH = 7.4) performed using an additively manufactured working electrode printed from the AuNP-CO (red), CO (blue) and commercial (black) filaments. **B)** Calibration plots for the detection of dopamine (5 – 100 μM) using differential pulse voltammetry and additively manufactured working electrodes printed from the AuNP-CO (red), CO (blue) and commercial (black) filaments.

increasing the concentration of dopamine, the AuNP-CO electrode produced a sensitivity for the detection of 0.268 μA μM^{-1} and a limit of detection (LOD) of 7.1 μM, compared to 0.14 μA μM^{-1} and LOD of 11.6 μM for the CO electrode, and 0.095 μA μM^{-1} and LOD of 17.2 μM for the commercial electrode. These significant improvements clearly show the effect of embedding AuNPs within a conductive filament. Importantly, this work shows a novel method for the development of conductive additive manufacturing filament containing metal nanoparticles through the synthesis within the bio-based oil employed as plasticiser, meaning that this chemical serves an electrochemical purpose as well as improving the low-temperature flexibility. We believe this filament has a chance to revolutionise the field of additive manufacturing electrochemistry, as the inclusion of metallic nanoparticles such as gold within the filament paves the way for alternative methods offering significant scope for further modification post print, whilst removing a costly and timely step from the manufacturing process.

4. Conclusions

Within this work we report the first production of a AuNP embedded conductive additive manufacturing filament. Through simple low-cost formation of AuNPs within castor oil, we show that this can be used not only as a plasticiser to improve low-temperature flexibility, but also as a key contributor to the electrochemical performance. The presence of AuNPs within the castor oil was confirmed through the colour change of the oil, UV–Vis spectroscopy, and TEM imaging of the nanoparticles. The AuNP modified castor oil was included withing a polymer composite at 10 wt%, alongside 25 wt% carbon black and 65 wt% recycled PLA. The inclusion of AuNPs within the castor oil did not negatively affect the low-temperature flexibility of the filament or the thermal stability as confirmed by TGA. The presence of AuNPs within the additively manufactured electrode was confirmed through EDX analysis. The electrodes were electrochemically tested against both outer and inner sphere probes and benchmarked against a CO only bespoke filament and a commercial alternative. It was seen that the AuNP-CO electrodes produced the best performance in all cases due to the excellent conductive properties and high surface area of the AuNPs, as they displayed the highest current values, lowest peak-to-peak separation in CVs and lowest Rct within EIS measurements. This translated into the electro-analytical response for dopamine where the AuNP-CO electrode produced a sensitivity of 0.268 μA μM^{-1}, compared to 0.14 μA μM^{-1} for the CO electrode and 0.095 μA μM^{-1} for the commercial electrode

highlighting the excellent performance of this filament. We foresee this report of the first precious metal nanoparticle embedded filament to open up various avenues of future research for the field of additive manufacturing electrochemistry.

Conflict of interest

There are no conflicts of interest to declare.

CRediT authorship contribution statement

Elena Bernalte: Writing – review & editing, Writing – original draft, Visualization, Validation, Supervision, Project administration, Methodology, Investigation, Formal analysis, Data curation, Conceptualization. **Robert D. Crapnell:** Writing – review & editing, Writing – original draft, Visualization, Validation, Supervision, Project administration, Methodology, Investigation, Formal analysis, Data curation, Conceptualization. **Rania El Azizi:** Formal analysis, Data curation. **Karen K.L. Augusto:** Writing – review & editing, Writing – original draft, Validation, Methodology, Investigation, Formal analysis, Data curation. **Craig E. Banks:** Writing – review & editing, Writing – original draft, Visualization, Validation, Supervision, Software, Resources, Project administration, Methodology, Investigation, Funding acquisition, Formal analysis, Data curation, Conceptualization.

Declaration of competing interest

The authors declare that they have no known competing financial interests or personal relationships that could have appeared to influence the work reported in this paper.

Acknowledgements

Supplementary materials

Supplementary material associated with this article can be found, in the online version, at doi:10.1016/j.apmt.2024.102578.

Data availability

Data will be made available on request.

References

[1] M. Attaran, Bus. Horiz. 60 (2017) 677.
[2] a) E. Bernalte, R.D. Crapnell, O.M. Messai, C.E. Banks, ChemElectroChem. 11 (2024) e202300576;
b) R.D. Crapnell, A. Garcia-Miranda Ferrari, M.J. Whittingham, E. Sigley, N. J. Hurst, E.M. Keefe, C.E. Banks, Sensors 22 (2022) 9521;
c) A.G.-M. Ferrari, N.J. Hurst, E. Bernalte, R.D. Crapnell, M.J. Whittingham, D. A. Brownson, C.E. Banks, Analyst 147 (2022) 5121;
d) R. Shergill, B. Patel, 2022. e) R.S. Shergill, C.L. Miller, B.A. Patel, Sci. Rep. 13 (2023) 339;
f) R.S. Shergill, B.A. Patel, ChemElectroChem. 9 (2022) e202200831.
[3] a) C. Kalinke, N.V. Neumsteir, G. de Oliveira Aparecido, T.V. de Barros Ferraz, P. L. Dos Santos, B.C. Janegitz, J.A. Bonacin, Analyst 145 (2020) 1207;
b) D.P. Rocha, R.G. Rocha, S.V. Castro, M.A. Trindade, R.A. Munoz, E.M. Richter, L. Angnes, Electrochem. Sci. Adv. 2 (2022) e2100136;
c) R.S. Shergill, B.A. Patel, ACS. Appl. Electron. Mater. 5 (2023) 5120;
d) R.S. Shergill, F. Perez, A. Abdalla, B.A. Patel, J. Electroanal. Chem. 905 (2022) 115994.
[4] R.D. Crapnell, C. Kalinke, L.R.G. Silva, J.S. Stefano, R.J. Williams, R.A.A. Munoz, J. A. Bonacin, B.C. Janegitz, C.E. Banks, Mater. Today 71 (2023) 73.
[5] P. Wuamprakhon, R.D. Crapnell, E. Sigley, N.J. Hurst, R.J. Williams, M. Sawangphruk, E.M. Keefe, C.E. Banks, Adv. Sustain. Syst. 7 (2023) 2200407.
[6] I.V. Arantes, R.D. Crapnell, M.J. Whittingham, E. Sigley, T.R. Paixão, C.E. Banks, ACS Appl. Eng. Mater. 1 (2023) 2397.
[7] R.D. Crapnell, I.V. Arantes, J.R. Camargo, E. Bernalte, M.J. Whittingham, B. C. Janegitz, T.R. Paixão, C.E. Banks, Microchimica Acta 191 (2024) 96.
[8] a) I.V. Arantes, R.D. Crapnell, E. Bernalte, M.J. Whittingham, T.R. Paixão, C. E. Banks, Anal. Chem. 95 (2023) 15086;
b) K.K. Augusto, R.D. Crapnell, E. Bernalte, S. Zighed, A. Ehamparanathan, J. L. Pimlott, H.G. Andrews, M.J. Whittingham, S.J. Rowley-Neale, O. Fatibello-Filho, Microchimica Acta 191 (2024) 375.
[9] C. Kalinke, R.D. Crapnell, P.R. de Oliveira, B.C. Janegitz, J.A. Bonacin, C.E. Banks, Glob. Challeng. 8 (2024) 2300408.
[10] E. Sigley, C. Kalinke, R.D. Crapnell, M.J. Whittingham, R.J. Williams, E.M. Keefe, B.C. Janegitz, J.A. Bonacin, C.E. Banks, ACS Sustain. Chem. Eng. 11 (2023) 2978.
[11] R.D. Crapnell, E. Sigley, R.J. Williams, T. Brine, A. Garcia-Miranda Ferrari, C. Kalinke, B.C. Janegitz, J.A. Bonacin, C.E. Banks, ACS Sustain. Chem. Eng. 11 (2023) 9183.
[12] a) J.R. Camargo, R.D. Crapnell, E. Bernalte, A.J. Cunliffe, J. Redfern, B. C. Janegitz, C.E. Banks, Appl. Mater. Today 39 (2024) 102285;
b) R.D. Crapnell, E. Bernalte, E. Sigley, C.E. Banks, RSC Adv. 14 (2024) 8108.
[13] A.D. Godwin, M. Kutz, William Andrew Appl. Sci. Publishers (2017).
[14] C. Iffelsberger, C.W. Jellett, M. Pumera, Small. 17 (2021) 2101233.
[15] R.D. Crapnell, I.V. Arantes, M.J. Whittingham, E. Sigley, C. Kalinke, B.C. Janegitz, J.A. Bonacin, T.R. Paixão, C.E. Banks, Green Chem. 25 (2023) 5591.
[16] a) J. Muñoz, M. Pumera, Chem. Eng. J. 425 (2021) 131433;
b) K. Partanen, Y. Pei, P. Hillen, M. Hassan, K. McEleney, G. Schatte, S.J. Payne, R. Oleschuk, Z. She, RSC Adv. 12 (2022) 33440;
c) M. Liao, Y. Yang, J. Ou, H. Yang, X. Dai, L. Zhong, J. Wen, Y. Jiang, L. Wang, Electrochem. Commun. 165 (2024) 107754.
[17] P. Thao Dao Vu, D. Nguyen Dac, T. Phuong Dinh, J. Solid State Electrochem. (2024).
[18] P. Karthika, S. Shanmuganathan, V. Subramanian, C. Delerue-Matos, Talanta 272 (2024) 125823.
[19] E.Da Silva, M.Da Silva, S. Meneghetti, G. Machado, M. Alencar, J. Hickmann, M. Meneghetti, J. Nanoparticle Res. 10 (2008) 201.
[20] S.F. Morais, M.G. da Silva, S.M. Meneghetti, M.R. Meneghetti, Comptes Rendus Chimie 18 (2015) 410.
[21] E.M. Richter, D.P. Rocha, R.M. Cardoso, E.M. Keefe, C.W. Foster, R.A. Munoz, C. E. Banks, Anal. Chem. 91 (2019) 12844.
[22] a) A.D. Viana, E.T.D. Nobrega, E.P. Moraes, A.O. Wanderley Neto, F.G. Menezes, L.H.S. Gasparotto, Mater. Res. Bull. 124 (2020) 110755;
b) M.B. Mensah, J.A.M. Awudza, P. O'Brien, R. Soc. Open Sci. 5 (2018) 180824.
[23] J. Liesenfeld, J.J. Jablonski, J.R.F. da Silva, A.A. Buenos, C.J. Scheuer, Int. J. Adv. Manuf. Technol. 130 (2024) 5813.
[24] Y. Wang, H. Zhao, H. Song, J. Dong, J. Xu, Microchimica Acta 187 (2020) 543.
[25] R.D. Crapnell, C.E. Banks, Talanta Open. 4 (2021) 100065.